Theoretical predictions for the effect of nebular emission on the broad-band photometry of high-redshift galaxies

Article (Published Version)

Monthly Notices
of the
ROYAL ASTRONOMICAL SOCIETY

MNRAS **435,** 2885–2895 (2013) doi:10.1093/mnras/stt1471
Advance Access publication 2013 September 17

Theoretical predictions for the effect of nebular emission on the broad-band photometry of high-redshift galaxies

Stephen M. Wilkins,[1,2]★ William Coulton,[2] Joseph Caruana,[2,3] Rupert Croft,[2,4] Tiziana Di Matteo,[2,4] Nishikanta Khandai,[4,5] Yu Feng,[4] Andrew Bunker[2] and Holly Elbert[2]

[1]*Astronomy Centre, Department of Physics and Astronomy, University of Sussex, Brighton BN1 9QH, UK*
[2]*Department of Physics, University of Oxford, Denys Wilkinson Building, Keble Road, OX1 3RH, UK*
[3]*Leibniz Institute for Astrophysics, An der Sternwarte 16, D-14482 Potsdam, Germany*
[4]*McWilliams Center for Cosmology, Carnegie Mellon University, 5000 Forbes Avenue, Pittsburgh, PA 15213, USA*
[5]*Department of Physics, Brookhaven National Laboratory, Upton, NY 11973, USA*

Accepted 2013 August 4. Received 2013 July 23; in original form 2013 June 13

ABSTRACT

By combining optical and near-IR observations from the *Hubble Space Telescope* with near-IR photometry from the *Spitzer Space Telescope*, it is possible to measure the rest-frame UV–optical colours of galaxies at $z = 4$–8. The UV–optical spectral energy distribution of star formation dominated galaxies is the result of several different factors. These include the joint distribution of stellar masses, ages and metallicities (solely responsible for the pure stellar spectral energy distribution), and the subsequent reprocessing by dust and gas in the interstellar medium. Using a large cosmological hydrodynamical simulation (*MassiveBlack-II*), we investigate the predicted spectral energy distributions of galaxies at high redshift with a particular emphasis on assessing the potential contribution of nebular emission. We find that the average (median) pure stellar UV–optical colour correlates with both luminosity and redshift such that galaxies at lower redshift and higher luminosity are typically redder. Assuming that the escape fraction of ionizing photons is close to zero, the effect of nebular emission is to redden the UV–optical $1500 - V_w$ colour by, on average, 0.4 mag at $z = 8$ declining to 0.25 mag at $z = 4$. Young and low-metallicity stellar populations, which typically have bluer pure stellar UV–optical colours, produce larger ionizing luminosities and are thus more strongly affected by the reddening effects of nebular emission. This causes the distribution of $1500 - V_w$ colours to narrow and the trends with luminosity and redshift to weaken. The strong effect of nebular emission leaves observed-frame colours critically sensitive to the redshift of the source. For example, increasing the redshift by 0.1 can result in observed-frame colours changing by up to ∼0.6. These predictions reinforce the need to include nebular emission when modelling the spectral energy distributions of galaxies at high redshift and also highlight the difficultly in interpreting the observed colours of individual galaxies without precise redshift information.

Key words: galaxies: high-redshift – galaxies: photometry.

1 INTRODUCTION

The availability of deep *Hubble Space Telescope* surveys utilizing the Advanced Camera for Surveys (ACS) and more recently Wide Field Camera 3 (WFC3) means it is now possible to routinely identify galaxies at very high redshift, with large (>50) samples identified to $z \approx 8$ (e.g. Bouwens et al. 2010a, 2011; Bunker et al. 2010; Finkelstein et al. 2010; Oesch et al. 2010a; Wilkins et al. 2010, 2011a; Lorenzoni et al. 2011, 2013; McLure et al. 2013; Schenker et al. 2013) and a few candidates now identified at $z > 10$ (e.g. Bouwens et al 2012; Coe et al. 2012; Oesch et al. 2012a, 2013; Ellis et al. 2013).

While *Hubble* ACS and WFC3 observations (which probe the rest-frame UV continuum at $z > 3$) alone allow us to learn a great deal about high-redshift galaxies, including the UV luminosity function (e.g. Bouwens et al. 2010a, 2011; Oesch et al. 2010a; Lorenzoni et al. 2011, 2013; Wilkins et al. 2011a; McLure et al.

★ E-mail: s.wilkins@sussex.ox.ac.uk

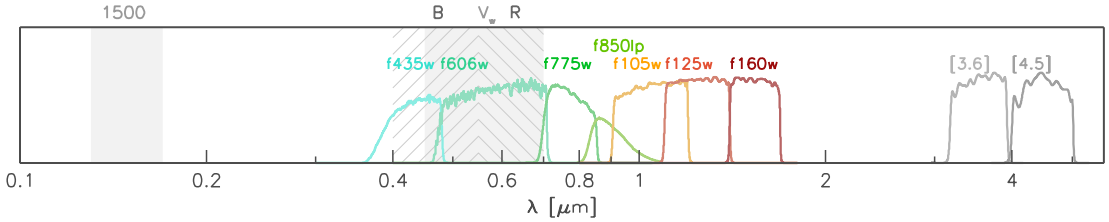

Figure 1. The transmission profiles of the various filters used throughout this study.

2013; Schenker et al. 2013), the UV continuum slope (e.g. Stanway, McMahon & Bunker 2005; Bouwens et al. 2010b, 2013; Bunker et al. 2010; Wilkins et al. 2011b, 2013a) and UV morphologies (e.g. Oesch et al. 2010b), by combining them with *Spitzer* Infrared Array Camera (IRAC) photometry it is possible to also probe the rest-frame optical emission. This is extremely difficult (given the lower sensitivity of the IRAC observations) for all but the brightest individual objects. However, by stacking large samples of galaxies together it becomes possible to robustly probe the average spectral energy distributions (SEDs) of even the faintest galaxies (e.g. Eyles et al. 2005; Labbé et al. 2010, 2012; González et al. 2011).

The UV/optical SED of a star formation dominated galaxy is affected by a complex mixture of different factors including the joint distribution of stellar masses, ages and metallicities, and dust and nebular emission, many of which are closely coupled. The large number of effects makes it difficult to ab initio interpret observations, especially at high redshift, where typically only broad-band photometry is available, in the context of any of these individual quantities.

In this paper, we use a state-of-the-art cosmological hydrodynamical simulation of structure formation (*MassiveBlack*-II) to investigate the UV–optical colours of high-redshift galaxies and in particular the effect of nebular emission thereupon. This paper is organized as follows: in Section 2 we discuss in turn the various factors affecting the rest-frame UV/optical colours of high-redshift galaxies. In Section 3, we present predictions from our large cosmological hydrodynamic simulation *MassiveBlack*-II. In Section 4, we describe how strong nebular emission makes robust estimates of galaxy stellar masses difficult. Finally, in Section 5 we present our conclusions. Magnitudes are calculated using the AB system (Oke & Gunn 1983). Throughout this work, we assume a Salpeter (1955) stellar initial mass function (IMF), i.e. $\xi(m) = \mathrm{d}N/\mathrm{d}m \propto m^{-2.35}$.

1.1 Filters used to probe the UV–optical SEDs

Throughout this work, we make use of several *Hubble* and *Spitzer* filters, including *Hubble*/ACS (B_{f435w}, V_{f606w}, i_{f775w} and z_{f850lp}), *Hubble*/WFC3 (Y_{f105w}, J_{f125w} and H_{f160w}) and *Spitzer*/IRAC ([3.6] and [4.5]) filters. We also introduce four rest-frame bandpasses (1500,[1] B,[2] V_w[3] and R[4]).[5] These rest-frame bandpasses allow us to consistently compare the properties of galaxies at different redshifts. The simple shape of these filters is chosen for convenience and the transmission profiles of all these filters are shown in Fig. 1. Fig. 2 shows the observed frame SED of a star forming galaxy at $z \in \{5.0, 5.9, 6.9, 8.0\}$ in relation to this filter set.

[1] Defined as $T_\lambda = [0.13 < \lambda/\mu\mathrm{m} < 0.17]^5$.
[2] Defined as $T_\lambda = [0.40 < \lambda/\mu\mathrm{m} < 0.55]^5$.
[3] Defined as $T_\lambda = [0.45 < \lambda/\mu\mathrm{m} < 0.70]^5$.
[4] Defined as $T_\lambda = [0.55 < \lambda/\mu\mathrm{m} < 0.70]^5$.
[5] Here we employ the Iverson bracket notation to define the bandpass, $[A] = 1.0$ when A is *True* and 0.0 otherwise.

2 FACTORS AFFECTING THE UV–OPTICAL COLOURS OF STAR-FORMING GALAXIES

The observed SEDs of galaxies are formed from the intrinsic stellar and AGN SEDs with reprocessing by dust and gas [both in the local interstellar medium (ISM) and intergalactic medium (IGM)]. The intrinsic SED of a stellar population (i.e. the *pure* stellar SED) is determined by the *joint* distribution of stellar masses, ages and metallicities. To demonstrate the effect of various changes on the star formation and metal enrichment histories, we utilize the PEGASE.2 (Fioc & Rocca-Volmerange 1997, 1999) stellar population synthesis (SPS) model. We first, in Sections 2.1 and 2.2, describe how the rest-frame intrinsic pure stellar UV–optical $1500 - V_w$ and optical $B - R$ colours are affected by the properties of the stellar population (distribution of masses, ages and metallicities). In Section 2.3, we extend this to include the effect of dust and in Section 2.4 we critically discuss the effect of nebular emission.

It is also important to stress that the predicted SED, for a given IMF, star formation history (SFH) and metal enrichment history, is also sensitive to the choice of the SPS model. In Appendix A, we investigate how changing the SPS model affects the predicted UV–optical colours.

2.1 Distribution of stellar mass and ages

The SEDs of individual stars vary strongly with both stellar mass and evolutionary stage (and therefore age). As such the intrinsic SED of a composite stellar population is predominantly determined by the joint distribution of stellar masses and ages. This, in turn, is determined by both the IMF and the SFH.

2.1.1 Star formation history

In general, stellar populations with protracted SFHs will contain a higher proportion of low-mass stars (as many of the original high-mass stars will have evolved off the main sequence) causing the SED of the population to redden relative to a younger population. The sensitivity of the UV/optical colours to the recent SFH can be seen in Fig. 3; this shows the sensitivity of both the rest-frame $1500 - V_w$ (UV–optical) and $B - R$ (optical) colours to the duration of previous (constant) star formation. Increasing the duration of previous star formation from $10 \rightarrow 1000$ Myr causes the pure stellar $1500 - V_w$ colour to redden by $\sim$1.4 mag. The effect on the optical $B - R$ colour is more subtle, with the colour increasing by only $\sim$0.2 mag as the previous duration of star formation is increased from $10 \rightarrow 1000$ Myr.

Assuming an increasing SFH, which is likely to be more representative of high-redshift star-forming galaxies (see for example the

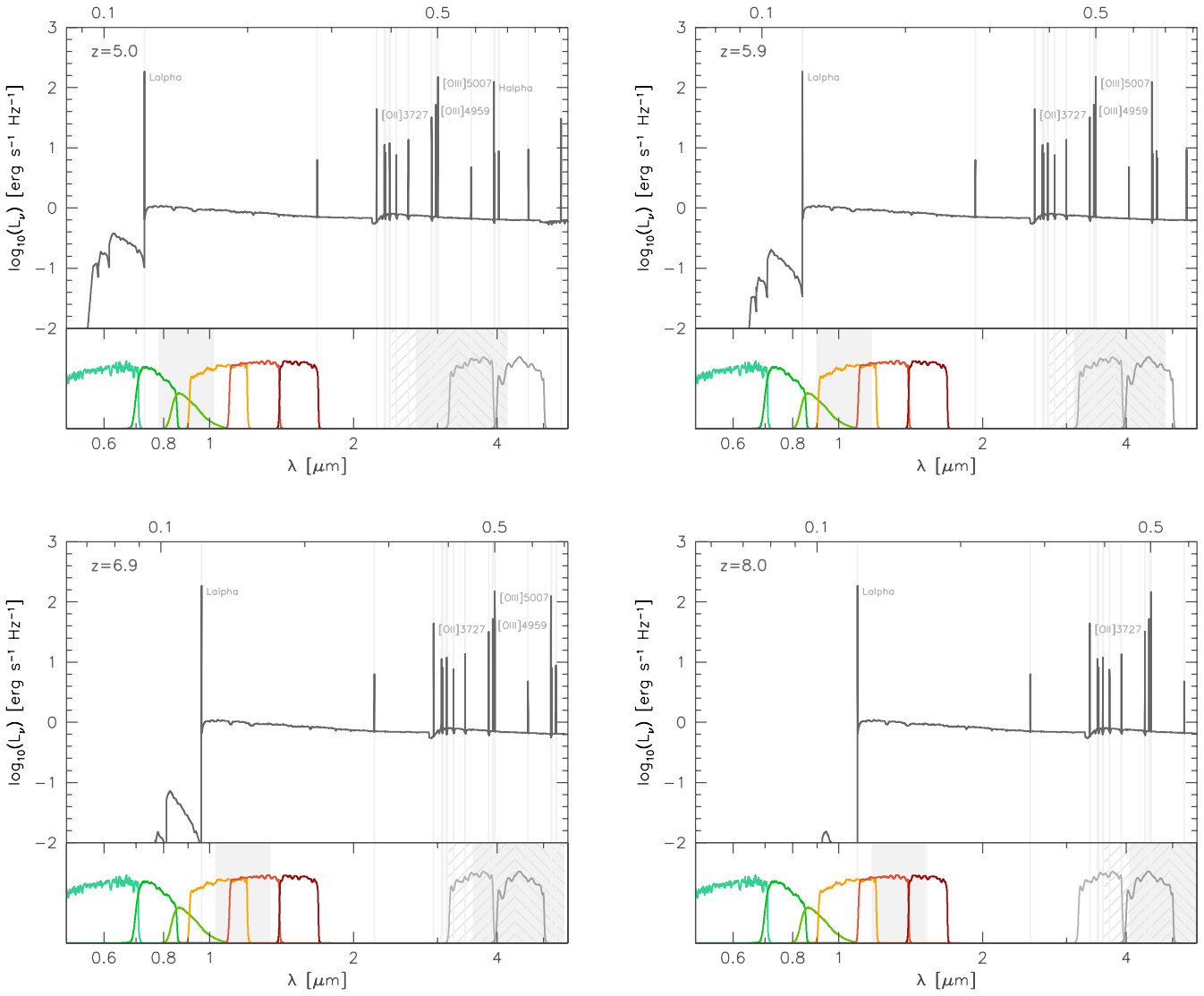

Figure 2. The SED of a stellar population which has formed stars at a constant rate for 100 Myr with $z = 0.004$ at $z \in \{5.0, 5.9, 6.9, 8.0\}$. For clarity only emission lines with $f_x > 0.2 \times f_{\mathrm{H}\beta}$ are shown (and only those with $f_x > f_{\mathrm{H}\beta}$ are labelled). The lower panel of each figure shows various *Hubble*/ACS (V_{f606w}, i_{f775w} and z_{f850lp}), *Hubble*/WFC3 (Y_{f105w}, J_{f125w} and H_{f160ww}) and *Spitzer*/IRAC ([3.6] and [4.5]) transmission curves. The shaded regions denote two artificial rest-frame bandpasses (1500 and V_w) and the two hatched regions denote the B and R bandpasses.

predictions of Finlator, Oppenheimer & Davé 2011), will suppress the evolution of the $1500 - V_w$ colour as the SED is dominated by the most massive stars. In contrast, if we instead consider the colour evolution of an instantaneous burst over the same time period ($10 \rightarrow 1000$ Myr), the $1500 - V_w$ and $B - R$ colours redden by $\sim$3.5 and $\sim$0.5 mag, respectively.

2.1.2 *Initial mass function*

Changing the choice of IMF will also affect the distribution of stellar masses. As such it can potentially have a significant effect on the colours of a stellar population. Changes to the low-mass ($<0.5\,\mathrm{M}_\odot$) end of the IMF have only a small effect on the shape of the SED as these stars contribute only a small fraction of the total luminosity (especially in the UV/optical) of actively star-forming galaxies. On the other hand, changes to the high-mass end will affect the mass distribution of luminous massive stars.

The high-mass IMF can be most simply parametrized as a power law, i.e. $\xi(m > 0.5\,\mathrm{M}_\odot) = \mathrm{d}N/\mathrm{d}m \propto m^{\alpha_2}$, where α_2 is the high-mass slope [which for the Salpeter (1955) IMF would be $\alpha_2 = -2.35$]. Increasing α_2 increases the relative proportion of very high mass stars resulting in a bluer $1500 - V_w$ colour, as can be seen in Fig. 4. Changing α_2 from -2.35 to -1.5 results in the pure stellar colour decreasing by $\sim$0.2 mag.

2.2 Metal enrichment history

Stars of similar mass and age with lower metallicities generally have higher effective temperatures and thus bluer UV/optical colours (see also Wilkins et al. 2012, 2013a). A stellar population with a similar SFH, but lower metallicity, will also then tend to have bluer UV–optical colours. This can be seen in Fig. 3, where the UV/optical colours ($1500 - V_w$, $B - R$) are shown for two metallicities ($Z \in \{0.02, 0.0004\}$). While (assuming the same duration of previous star formation) the high-metallicity population is always redder,

the difference is sensitive to the previous star formation duration (and thus the distribution of stellar masses and ages).

2.3 Dust

Throughout the UV to NIR dust acts to preferentially absorb light at shorter wavelengths. One effect of dust is then to cause the observed colour to redden relative to the intrinsic colour, i.e. $(m_a - m_b)^{\rm obs} = (m_a - m_b)^{\rm int} + E(B-V)(k_a - k_b)$, where $\lambda_a < \lambda_b$, $E(B-V) \geq 0.0$ and $k_a > k_b$. The extent of the reddening due to dust is then a product of the attenuation/reddening curve $k(\lambda)$ and a measure of the total attenuation [often expressed by the colour excess $E(B-V)$].

Assuming a Small Magellanic Cloud-like curve (Pei 1992), which is favoured at high redshift by recent observations (e.g. Oesch et al. 2012b), an optical attenuation of $A_V = 0.4$ mag (which corresponds to $A_{1500} \approx 1.76$ mag) will redden the $1500 - V_w$ and $B - R$ colours by $\approx$1.36 and $\approx$0.15, respectively (assuming no distinction in the effect of dust between nebular and stellar emission).

If instead we assume a Calzetti et al. (2000) starburst curve (and again assume no distinction in the effect of dust between nebular and stellar emission), the same V-band attenuation (i.e. $A_V = 0.4$ mag, which corresponds to $A_{1500} \approx 1.03$ mag) reddens the $1500 - V_w$ colour by $\approx$0.63 mag and the $B - R$ colour by only $\approx$0.12 mag. However, Calzetti et al. (2000) found that the nebular emission of intensely star-forming galaxies is more strongly affected by dust than the stellar emission (at the same wavelength) with the relationship between the colour excess of the nebular and stellar emission of $E(B-V)_{\rm stellar} = (0.44 \pm 0.03) \times E(B-V)_{\rm nebular}$. A significant consequence of assuming the Calzetti et al. (2000) is that there is no longer a unique mapping between the intrinsic and observed colours for a given attenuation.

While in this work we are more concerned with the effect of nebular emission on the intrinsic photometry, it is however worth noting that the similar consequences of dust attenuation, the star formation history and metallicity make interpreting the observed broad-band colours of stellar populations in the context of these quantities extremely challenging.

2.4 Nebular emission

Ionizing radiation, which is produced predominantly by hot, young ($<$10 Myr), massive stars ($>30\,{\rm M}_\odot$),[6] is potentially reprocessed by gas in the ISM into nebular (line and continuum) emission. At high redshift ($z > 4$), galaxy formation models (see Section 3) suggest that virtually all galaxies continue to actively form, or have recently formed, stars.[7] Assuming that the escape fraction of ionizing photons (X_f) is small, these galaxies are likely to contain strong nebular line emission.

To include the effect of nebular emission on our predictions, we use the number of ionizing photons predicted (by PEGASE.2) to determine the fluxes in the hydrogen recombination lines. Fluxes in *non*-hydrogen lines are determined using the metallicity-dependent conversions of Anders & Fritze-v. Alvensleben (2003).[8] Throughout this analysis, we assume that the escape fraction (X_f) is zero. This assumption allows us, when combined with the pure stellar colours, to explore the full range of potential colours.

2.4.1 *Effect on rest-frame UV–optical colours*

Due to the number of strong emission lines (e.g. O[II], Hβ, O[III] and Hα) in the rest-frame optical, unless the bandpass used to probe the UV encompasses Lyman α, the effect of nebular emission will be to redden the UV–optical colour relative to that of the pure stellar colour. This can be seen in Fig. 3 where both the pure stellar and the stellar with nebular emission colours are shown (as a function of previous duration of star formation).

For a 100 Myr duration of previous constant star formation and $Z = 0.02$, the effect of including nebular emission is to redden the $1500 - V_w$ colour by $\sim$0.3 (see Fig. 3). However, the relative effect of nebular emission changes with both metallicity and previous star formation duration. For protracted ($>$1000 Myr) constant star formation, the effect decreases to $\sim$0.1 mag (if there has been no star formation for $>$10 Myr, the contribution of nebular emission will also fall to virtually zero). This variation is predominantly due to the sensitivity to the ratio of ionizing photon flux to the optical flux which is itself sensitive to the (joint) distribution of stellar masses, ages and metallicities. The variation with metallicity is in part also due to the metallicity-dependent line ratios.

The inclusion of nebular emission can (for actively star-forming populations) also dramatically modify the trend with the high-mass slope of the IMF compared to the pure stellar case (Section 2.1.2), as can be seen in Fig. 4. When nebular emission is included, the trend between the $1500 - V_w$ colour and high-mass slope reverses: stellar populations with shallower IMFs (high-mass biased) have redder $1500 - V_w$ colours. This is again a result of the increased proportion of massive hot stars which produce large amounts of ionizing radiation.

2.4.2 *Redshift sensitivity and effect on observed colours*

The effect of nebular emission on observed-frame colours is critically sensitive to both the filter transmission curve and the redshift of the source. Small changes in redshift can leave strong emission lines in adjacent bands, dramatically affecting the observed colour.

This can be seen in Fig. 5, where the $X-[3.6]$ (where $X \in \{z_{f850lp}, Y_{f105w}, J_{f125w}, H_{f160w}\}$) and $[3.6]-[4.5]$ colours (both from the pure stellar SED and the stellar+nebular) of a young star-forming stellar population (100 Myr continuous star formation) are shown as a function of redshift (Fig. 2 also shows the SED of a stellar population forming stars for 100 Myr along with the transmission functions of the various observed-frame filters). For example, at $z = 5-5.3$ there are no strong emission lines within the IRAC [3.6] bandpass, thus leaving the $X-[3.6]$ colour virtually unchanged relative to that for a pure stellar SED (unless the X filter encompasses Lyman α). In contrast, at $z < 5$ and $z > 5.3$ the IRAC [3.6] filter includes strong emission lines (O[III] and Hβ, or Hα, respectively). This results in an extremely strong sensitivity to the redshift. An increase in redshift of 0.1 (i.e. $z = 5.0 \rightarrow 5.1$) can decrease the $X-[3.6]$ colour by 0.5[9] while correspondingly increasing the $[3.6]-[4.5]$ colour by 0.7. A similar situation occurs at $z \approx 7$ as the [O III] and Hβ lines move out of the [3.6] band into

[6] This also makes the presence of nebular line emission a powerful diagnostic of unobscured ongoing star formation.

[7] Even if this were not the case, it is likely that many of the galaxies currently *observed* (at these redshifts) would be actively forming stars by virtue of being rest-frame UV selected.

[8] PEGASE.2 can, without modification, output emission line fluxes; however, it does not take account variations in the line ratios due to metallicity.

[9] $z = 5$ is a declining inflexion point for the $X-[3.6]$ colour.

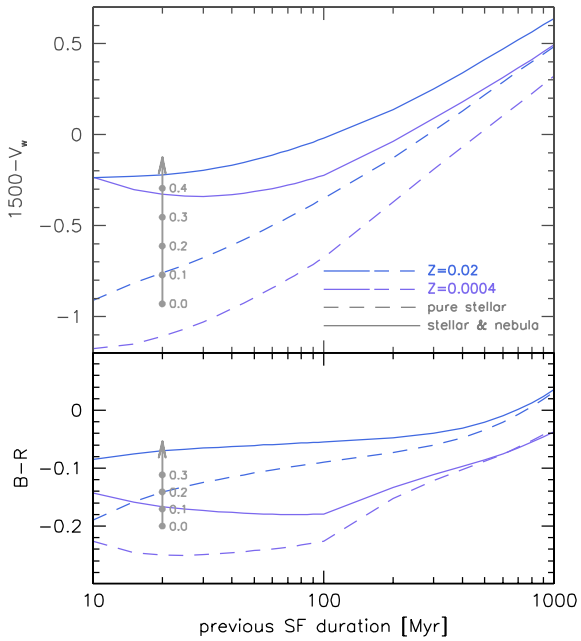

Figure 3. The predicted (using the PEGASE.2 SPS code) UV–optical ($1500 - V_w$) and optical $B - R$ (lower panel, note the difference in scale) colours as a function of the previous duration of (constant) star formation. Colours are shown for both metallicities ($Z \in \{0.02, 0.0004\}$) and for both a pure stellar SED (dashed lines) and the SED including a nebular contribution (solid lines). The two arrows show the effect of $A_V = 0.5$ dust attenuation (with labels denoting intermediate values of A_V) assuming the Calzetti et al. (2000) reddening law.

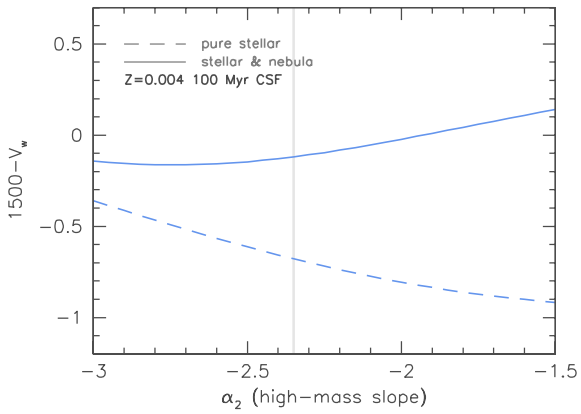

Figure 4. The predicted UV–optical ($1500 - V_w$) colour as a function of the choice of IMF high-mass slope (α_2) for both a pure stellar SED (dashed lines) and the SED including a nebular contribution (solid lines). In each case, a metallicity of $Z = 0.004$ and a 100 Myr duration of previous star formation are assumed. The vertical line denotes the Salpeter (1955) IMF ($\alpha_2 = -2.35$).

the [4.5] band. The [3.6]−[4.5] colour (which probes the rest-frame optical at $z = 4-8$) also experiences significant variation as a function of redshift, as shown in the lower panel of Fig. 5. Specifically, both $z = 5$ and $z = 6.9$ are approximately rising inflexion points, again caused by the shifting locations of the various strong emission lines.

This highlights that interpreting the observed colours of galaxies with strong emission lines is extremely challenging without precise knowledge of the redshift (or redshift distribution).

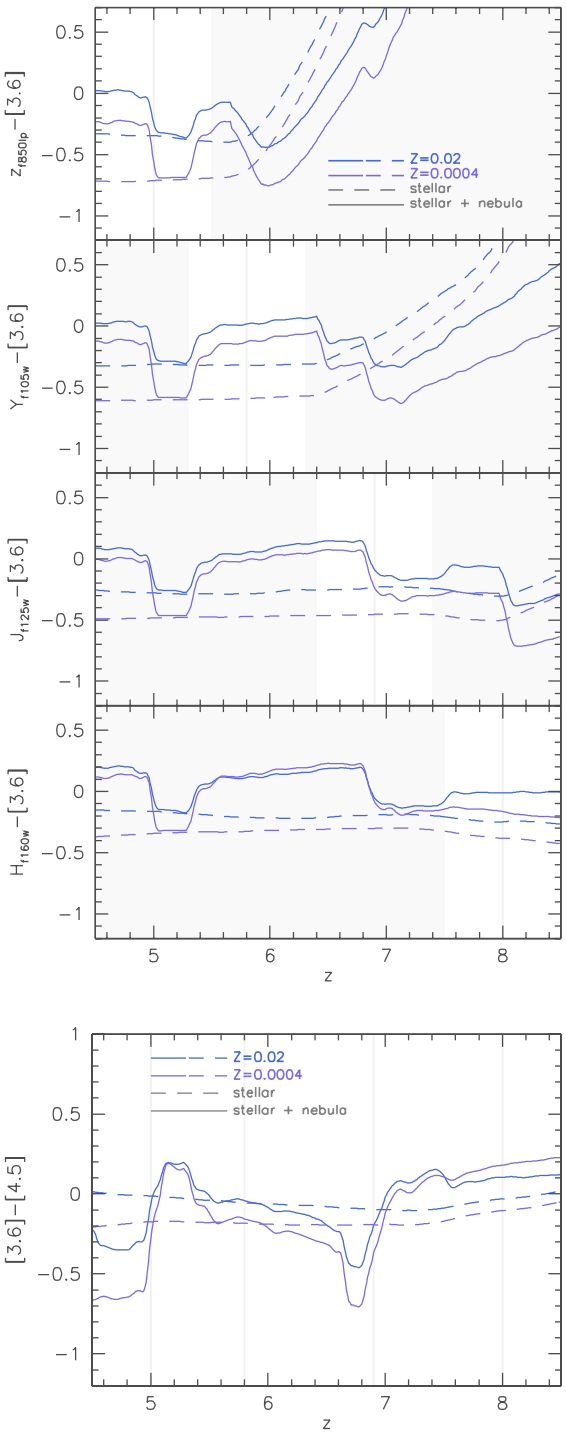

Figure 5. The predicted observed-frame $X-[3.6]$ (where $X \in \{z_{f850lp}, Y_{f105w}, J_{f125w}, H_{f160w}\}$) and [3.6]−[4.5] colours as a function of redshift assuming 100 Myr previous duration of star formation for two (stellar) metallicities ($Z = 0.02$ and 0.0004). The dashed lines show the result if only stellar emission is included, while the solid lines show the effect of including nebular emission (continuum and line emission).

3 PREDICTIONS FROM GALAXY FORMATION SIMULATIONS

The preceding analysis demonstrated that the observed-frame optical/NIR colours of high-redshift galaxies can be extremely sensitive to nebular emission. By using a galaxy formation model to predict

both the star formation and metal enrichment histories, we can predict the stellar SEDs and nebular (line and continuum) emission and thus the intrinsic observed colours.

3.1 *MassiveBlack*-II

We make use of a state-of-the-art cosmological hydrodynamic simulation of structure formation: *MassiveBlack*-II (for a more detailed description of this simulation, see Khandai et al., in preparation). The *MassiveBlack*-II simulation is performed using the cosmological TreePM smooth particle hydrodynamics code P-GADGET, a hybrid version of the parallel code GADGET2 (Springel 2005) tailored to run on the new generation of petaflop-scale supercomputers. *MassiveBlack*-II includes $N_{\rm par} = 2 \times 1792^3 \approx 11.5$ billion particles in a volume of $10^6\,{\rm Mpc}^3\,h^{-3}$ ($100\,{\rm Mpc}\,h^{-1}$ on a side) and includes not only gravity and hydrodynamics but also additional physics for star formation (Springel & Hernquist 2003), metal enrichment, black holes and associated feedback processes (Di Matteo et al. 2008, 2012).

3.1.1 *Properties of galaxies in the simulation*

A detailed overview of the properties of galaxies (galaxy stellar mass functions, luminosity functions, etc.) in the simulation is presented in Khandai et al. (in preparation). Nevertheless, it is useful to present predictions for the properties which directly influence the UV–optical colours of galaxies, i.e. the star formation and metal enrichment histories.

Instead of presenting the full star formation and metal enrichment histories, in Fig. 6 we show the median mass-weighted stellar age in bins of intrinsic UV luminosity and in Fig. 7, the median mass-weighted stellar metallicity, in both cases for a range of redshifts ($z \in \{5, 6, 7, 8, 9, 10\}$). The redshift trends can be seen more clearly in Fig. 8, where the evolution of median mass-weighted stellar age and metallicity for galaxies with $-20.5 < M_{1500} < -18.5$ is shown.

Fig. 6 reveals only a very weak correlation between UV luminosity suggesting that any correlation in the predicted UV–optical colours is unlikely to be dominated by variations in the SFH. Fig. 7 on the other hand reveals a strong correlation between the mass-weighted stellar metallicity and the UV luminosity. Both quantities do however show strong variation with redshift (as can be seen clearly in Fig. 8).

3.1.2 *Stellar SEDs*

The stellar SEDs of galaxies are generated by combining the SEDs of individual star particles taking account of their metallicity and age using the SPS model PEGASE.2 and assuming a Salpeter (1955) IMF. As noted previously, the SED predicted from a given star formation and metal enrichment history is sensitive to the choice of the SPS model. In Appendix , we consider the effect of alternative SPS models on the SED of galaxies predicted by the simulation.

3.1.3 *Nebular emission and dust attenuation*

Nebular emission is included in the simulated SEDs using the same prescription described in Section 2.4. We take the ionizing flux predicted from the stellar SED and determine the fluxes in the various hydrogen recombination lines assuming that the escape fraction is zero. We then use the calibrations of Anders & Fritze-v. Alvensleben (2003) to determine the fluxes in the non-hydrogen lines. We also use PEGASE.2 to predict the contribution of nebular continuum emission (though this is typically very small except in extreme cases). For the results presented here, we do not include dust attenuation concentrating solely on the intrinsic photometry.

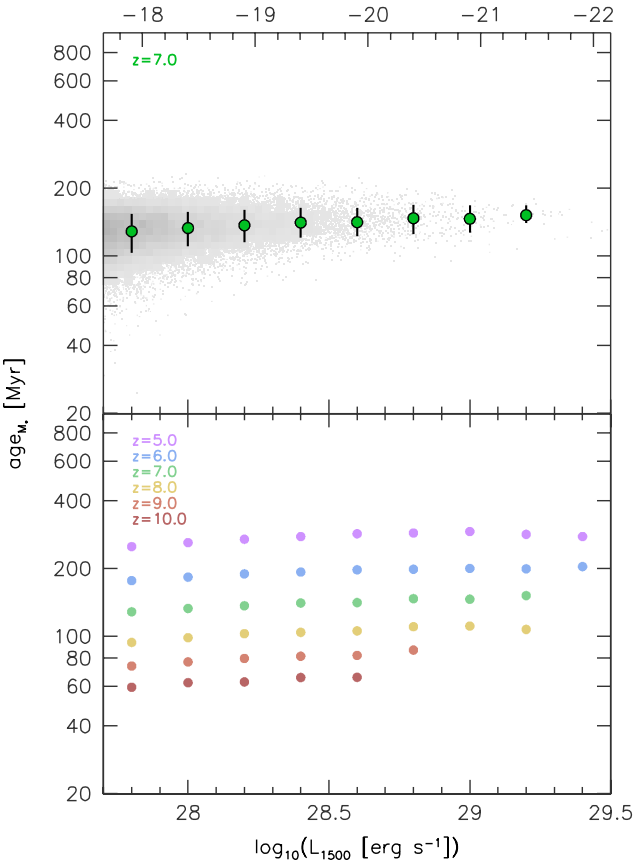

Figure 6. The mass-weighted stellar age as a function of the intrinsic UV luminosity predicted by the *MassiveBlack*-II simulation. The upper panel shows both a density plot (with shading denoting the number of galaxies) and the median age (and 16th−84th percentile range) in several luminosity bins at $z = 7$. The shade of the density plot denotes the number of galaxies contributing to each bin on a linear scale. Where there are fewer than 25 galaxies contributing to each bin on the density plot, the galaxies are plotted individually. The lower panel shows only the median age as a function of luminosity but for a range of redshifts ($z \in \{5, 6, 7, 8, 9, 10\}$).

3.2 Stellar colours

The top panel of Fig. 9 shows the median rest-frame pure stellar $1500 - V_w$ colour as a function of the intrinsic UV luminosity ($M_{1500,\,\rm int}$) for galaxies at $z \in \{5, 6, 7, 8, 9, 10\}$. The $1500 - V_w$ colour is correlated, albeit weakly, with the UV luminosity with the colour reddening by $\sim$0.15 as $M_{1500,\,\rm int} = -18 \rightarrow -20$ (at $z = 7$). The $1500 - V_w$ colour is also strongly correlated with redshift as can be seen more clearly in Fig. 10, where the median pure stellar colour (of galaxies with $-20.5 < M_{1500} < -18.5$) is shown as a function of redshift. For example, the median $1500 - V_w$ colour increases by $\sim$0.5 from $z = 8 \rightarrow 5$.

The distribution of pure stellar colours for galaxies with $-20.5 < M_{1500} < -18.5$ is shown in Fig. 11. The 16th−84th percentile range is 0.15 mag though this increases slightly to lower redshift.

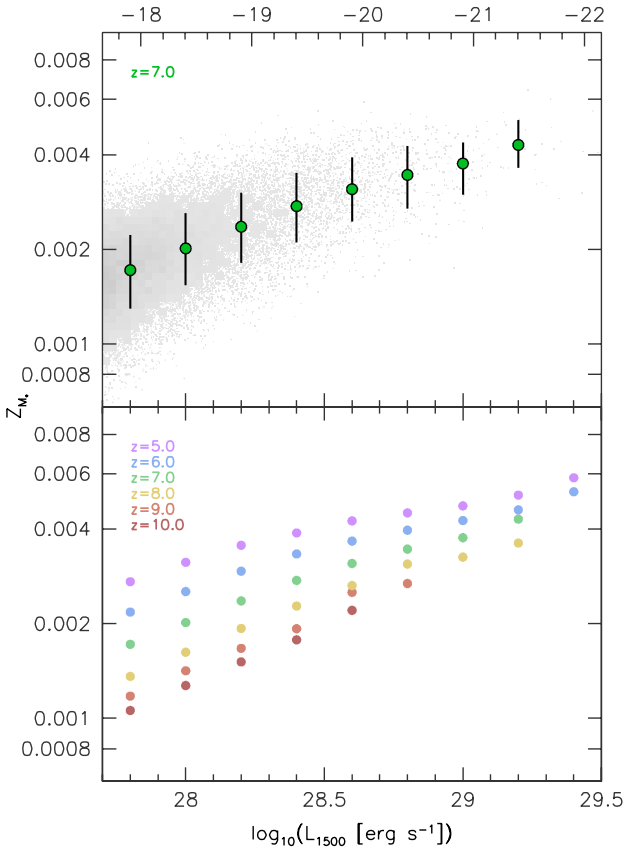

Figure 7. The mass-weighted stellar metallicity as a function of the intrinsic UV luminosity predicted by the *MassiveBlack*-II simulation. The upper panel shows both a density plot (with shading denoting the number of galaxies) and the median metallicity (and 16th–84th percentile range) in several luminosity bins at $z = 7$. The shade of the density plot denotes the number of galaxies contributing to each bin on a linear scale. Where there are fewer than 25 galaxies contributing to each bin on the density plot, the galaxies are plotted individually. The lower panel shows only the median stellar metallicity as a function of luminosity but for a range of redshifts ($z \in \{5, 6, 7, 8, 9, 10\}$).

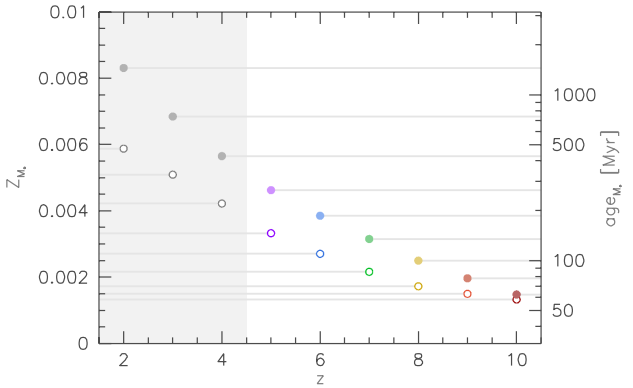

Figure 8. The evolution with redshift of the simulated average (median) mass-weighted age (right-hand axis) and stellar metallicity of galaxies in the simulation with $-20.5 < M_{1500} < -18.5$.

The correlation with redshift is driven by the variation in both the average star formation and metal enrichment histories of galaxies (as shown in Fig. 8) while the correlation with luminosity is driven predominantly by the variation in the metal enrichment history.

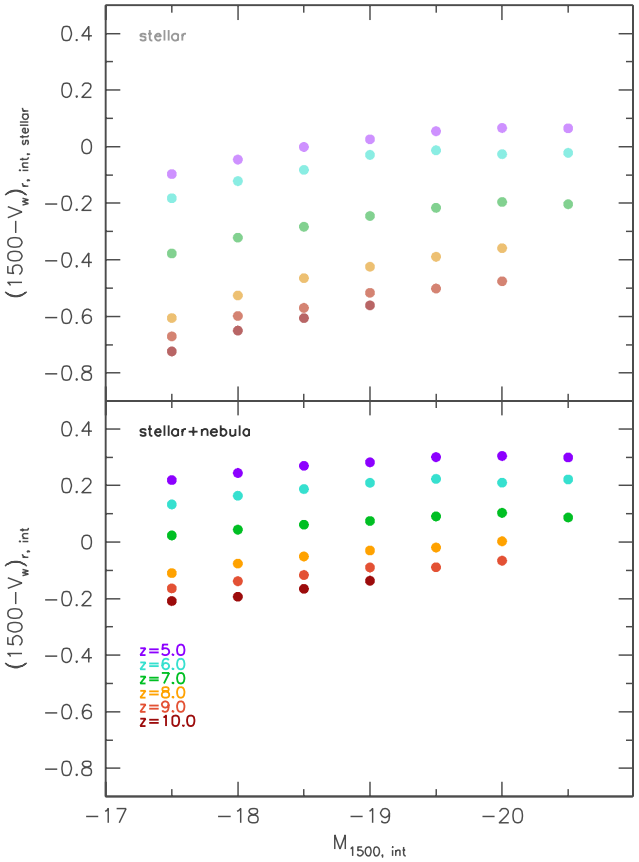

Figure 9. The simulated average (median) intrinsic (i.e. with no dust attenuation) rest-frame $1500 - V_w$ colours of galaxies as a function of luminosity for galaxies at $z \in \{5, 6, 7, 8, 9, 10\}$. The upper panel shows only the pure stellar colours while the lower panel shows the average colour including the effects of nebular emission.

3.3 The effect of nebular emission

As noted in Section 2.4, the effect of nebular emission will, by adding additional flux in the V_w band, have the result of reddening the rest-frame $1500 - V_w$ colour relative to the pure stellar colour. This is shown for our simulated galaxies in Figs 9 and 10.

As can be seen in Figs 9 and 10, the effect of adding nebular emission is to flatten the correlation between the $1500 - V_w$ colour and the UV luminosity and redshift. The median $1500 - V_w$ colour including nebular emission only reddens by ∼0.05 from $M_{1500,\,\mathrm{int}} = -18 \rightarrow -20$ (at $z = 7$). This is because the relative strength of nebular emission is inversely correlated with both stellar metallicity and age. Those galaxies with bluer stellar colours, which are indicative of more recent star formation or lower metallicity (which are more common at higher redshift and lower luminosity), will then have stronger nebular emission and consequently will be reddened by nebular emission more than those with redder stellar colours. This has the effect of diminishing the correlation of the $1500 - V_w$ colour with redshift and luminosity. The median $1500 - V_w$ colour including nebular emission only reddens by ∼0.1 from $M_{1500,\,\mathrm{int}} = -18 \rightarrow -20$ and by ∼0.3 from $z = 8 \rightarrow 5$ (cf. 0.1 and 0.3 for the pure stellar case, respectively).

3.3.1 The distribution of colours

Because galaxies with bluer pure stellar galaxies typically have lower metallicities and/or ages (and consequently stronger nebular

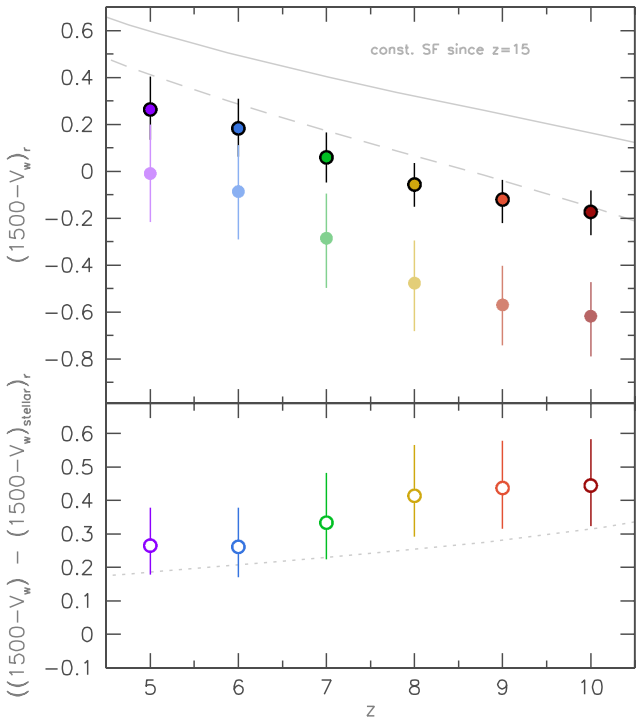

Figure 10. The redshift evolution of the median rest-frame $1500 - V_w$ colour (points) and 16th−84th percentile range for both the simulated pure stellar SED and the simulated SED including nebular emission (outlined points) for galaxies with $-20.5 < M_{1500} < -18.5$. The lower panel shows the difference between the pure stellar colour and the colour including nebular emission. The dashed and solid lines show the prediction (using the PEGASE.2 SPS model) assuming constant star formation since $z = 15$ for the pure stellar and stellar with nebular emission SEDs, respectively.

emission), the inclusion of nebular emission reduces the scatter in the $1500 - V_w$ colour (as measured by the 16th−84th percentile range), as can be seen in Fig. 11. At $z = 8$ this reduces the scatter (as measured by the 16th−84th percentile range) by almost a factor of 2 while at lower redshift it is less important.

3.3.2 *The distribution equivalent widths*

One alternative measure of the relative strength of nebular emission is the distribution of the equivalent widths of the prominent Hα and [O III]λ5007 emission lines. These are shown in Fig. 12 and follow a similar pattern to the distribution of colour increments shown in Fig. 11.

3.3.3 *The effect on observed colours*

As noted in Section 2.4, the effect of nebular emission on observed-frame colours is strongly sensitive to both the choice of filters and the redshift of the source. Even a small change in redshift can have a dramatic effect on the observed colour. Fig. 13 shows the average simulated (for galaxies with $-20.5 < M_{1500} < -18.5$) observed-frame $X-[3.6]$ and $[3.6]-[4.5]$ colours for redshift ranges centred on the median redshift of observed drop-out samples (see Labbé et al. 2010, 2012; González et al. 2011) – V_{f606w}-band drop-out: $\langle z \rangle = 5.0$, i_{f775w}: $\langle z \rangle = 5.9$, z_{f850lp}: $\langle z \rangle = 6.9$ and Y_{f105w}: $\langle z \rangle = 8.0$. In each case, the X filter is chosen (from the available *Hubble* ACS and WFC3 filters) such that it *approximately* probes the rest-frame UV continuum at 1500 Å. Therefore, we

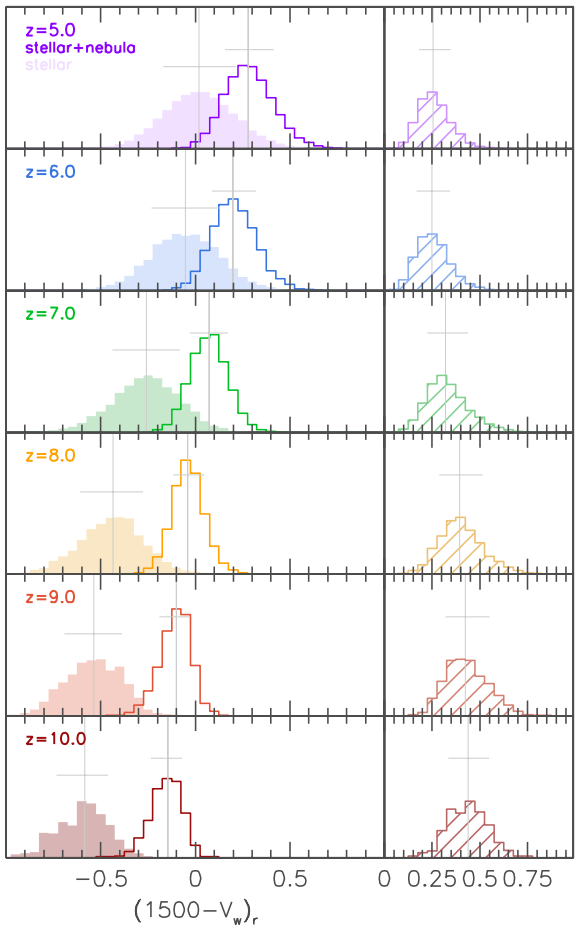

Figure 11. Left-hand panels: the distribution of both pure stellar (shaded histogram) and stellar with nebular (line histogram) intrinsic rest-frame $1500 - V_w$ colours for galaxies with $-20.5 < M_{1500} < -18.5$ at $z \in \{5, 6, 7, 8, 9, 10\}$. Right-hand panels: the distribution of colour residuals. In each case, the vertical and horizontal lines denote the median and 16th−84th percentile range of the distribution, respectively.

use $z \approx 5 \rightarrow z_{f850lp}$, $z \approx 6 \rightarrow Y_{f105w}$, $z \approx 7 \rightarrow J_{f125w}$ and $z \approx 8 \rightarrow H_{f160w}$.

The trends seen in Fig. 13 closely reflect those demonstrated in Section 2.4 (and seen in Fig. 5). We see that at $z \approx 5$ and $z \approx 7$ the observed colours are particularly sensitive to the redshift, with changes in redshift of 0.1 changing the *average* observed colours by up to 0.3 mag.

Stark et al. (2012, hereafter S12) studied the observed-frame $[3.6] - [4.5]$ colours of a spectroscopically confirmed sample of galaxies at $3 < z < 7$. S12 compare the $[3.6] - [4.5]$ colour distribution at $3.8 < z < 5.0$ (where Hα emission, if present, will contaminate the [3.6] filter) with those at $3.1 < z < 3.6$ (where there are expected to be no strong nebular emission lines in either the [3.6] or [4.5] filter) finding that the $[3.6] - [4.5]$ colour at $3.8 < z < 5.0$ is 0.33 mag bluer than at $3.1 < z < 3.6$. This is interpreted as being due to the presence of nebular line emission. This closely matches our prediction at $4.5 < z < 4.9$ where we find the effect of nebular emission results in the observed $[3.6] - [4.5]$ colour being 0.25 mag bluer than the pure stellar colour. S12 also attempt to determine the increase in the [3.6] flux due to nebular emission at $3.8 < z < 5.0$ by comparing the observed [3.6] flux with that expected from the best-fitting stellar continuum models, and find an increase in the [3.6] flux ($[3.6]_{\rm neb} - [3.6]_{\rm stellar} = -0.27$ mag)

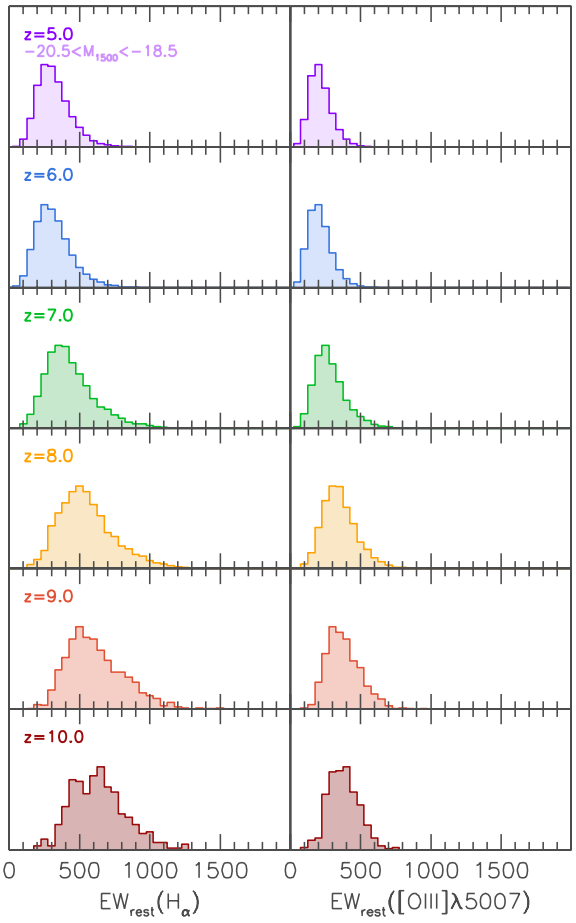

Figure 12. The distribution of rest-frame intrinsic equivalent widths of the Hα (left) and [O III]λ5007 predicted by the simulation for galaxies with $-20.5 < M_{1500} < -18.5$ at $z \in \{5, 6, 7, 8, 9, 10\}$.

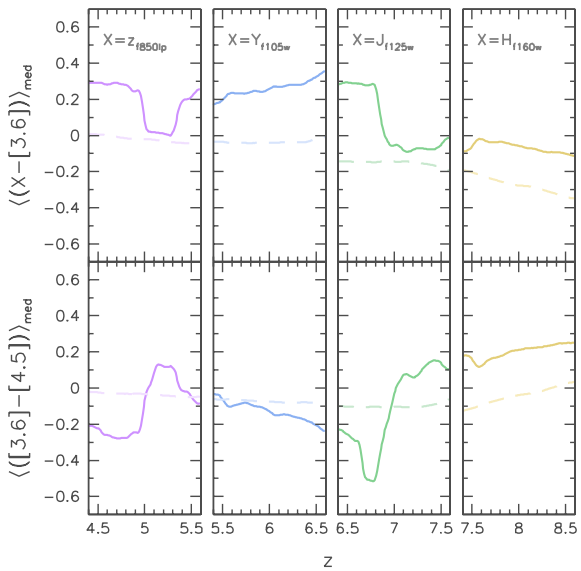

Figure 13. The simulated observed-frame $X-[3.6]$ (top panels, $X \in \{z_{f850lp}, Y_{f105w}, J_{f125w}, H_{f160w}\}$) and [3.6]−[4.5] colours as a function of redshift across a narrow range centred on the snapshot redshift. The dashed and solid lines again denote the colours for the pure stellar SEDs and those including nebular emission, respectively.

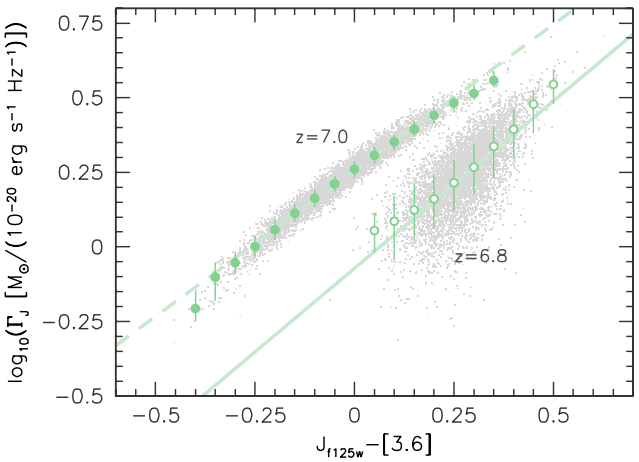

Figure 14. The simulated observed-frame $J_{f125w} - [3.6]$ colours and J_{f125w}-band mass-to-light ratios of galaxies at $z = 6.8$ and $z = 7.0$ with $-20.5 < M_{1500} < -18.5$. The two straight lines denote simple linear fits to the two sets of simulations.

consistent with our predictions at $4.5 < z < 4.9$ ($[3.6]_{\rm neb} - [3.6]_{\rm stellar} = -0.29$ mag).

4 THE EFFECT ON STELLAR MASS ESTIMATES

We have seen that the effect of nebular emission is to typically redden the observed colour probing the rest-frame UV–optical relative to the pure stellar colour. For individual galaxies at $z \approx 7$, this can be as large as +0.6 mag with the average at $z = 6.8$ being +0.4 mag for J_{f125w} −[3.6]. The effect is also strongly dependent on the redshift and choice of observed filters with changes in the redshift of as little as ±0.1 able to change the observed colours by >0.3 mag.

Because accurate estimates of the stellar mass-to-light ratio require a measurement of the shape rest-frame UV–optical SED (e.g. Wilkins et al. 2013b), the effect of nebular emission can introduce a large bias, particularly where the redshift is not known accurately. The exact size of the effect of nebular emission on stellar mass estimates however depends on various factors including the method used to measure the mass-to-light ratio, the redshift.

As a simple illustration, we consider the case where the stellar mass-to-light ratio is measured using a single colour (e.g. Taylor et al. 2011; Wilkins et al. 2013b). Fig. 14 shows the relationship between the observed-frame J_{f125w} −[3.6] colours and J_{f125w}-band stellar mass-to-light ratios of galaxies at $z = 6.8$ and $z = 7.0$. In both cases, the J_{f125w} −[3.6] colour is correlated with the mass-to-light ratio (though the correlation is much stronger at $z = 7.0$ where the effect of nebular emission is smaller than at $z = 6.8$); however, for the same observed colour the average mass-to-light ratio at $z = 7.0$ is ∼0.25 dex (1.8 times) larger. That is, were the redshift erroneously assumed to be at $z = 7.0$ instead of the true redshift of $z = 6.8$, the stellar mass-to-light ratio would be overestimated by around ∼0.25 dex.

5 CONCLUSIONS

We have explored the evolution of the rest-frame UV/optical (and observed-frame near-IR) colours of high-redshift galaxies ($z = 5-10$) predicted by our large cosmological hydrodynamical simulation *MassiveBlack*-II.

We find that the median rest-frame *pure* stellar UV–optical ($1500 - V_w$) colour is correlated with both luminosity and redshift. The $1500 - V_w$ colour reddens by $\sim$0.2 as the luminosity increases from $M_{1500} = -18$ to -20 (at $z = 7$) and by $\sim$0.5 from $z = 8$ to $z = 5$. In both cases, this reflects the trend of increasing ages and metallicities with luminosity and to lower redshift.

However, when nebular emission is included, these correlations weaken. The $1500 - V_w$ colour reddens by only $\sim$0.3 mag as $z = 8 \rightarrow 5$ and $\sim$0.1 mag as $M_{1500} = -18 \rightarrow -20$. This occurs because galaxies with very blue stellar colours (indicative of galaxies with recent star formation or low metallicity) typically have stronger nebular emission causing their colours to redden by a greater relative amount.

The effect of nebular emission on observed-frame colours is very sensitive to both the choice of filters and redshift. For example, at $z = 7.0$, nebular emission only reddens the observed $J_{f125w} - [3.6]$ colour by, on average, $\sim$0.1 mag while at $z = 6.8$ it reddens the $J_{f125w} - [3.6]$ colour by $\sim$0.45 mag (i.e. a difference of $\sim$0.35 mag). Similarly, at $z = 7.1$, nebular line emission causes the $[3.6]-[4.5]$ to redden by $\sim$0.2 mag, while at $z = 6.8$ it causes the $[3.6]-[4.5]$ colour to shift blueward by $\sim$0.4 mag (a net difference of $\sim$0.6 mag).

This strong sensitivity of observed colours to the redshift makes interpreting the colours of individual objects extremely difficult unless precise redshifts are known.

While the general trends we observe hold true irrespective of the choice of the IMF and SPS model, both these factors can strongly affect the predicted colours. For example, utilizing the Maraston (2005) model yields stellar colours between 0.1and0.3 mag redder than the PEGASE.2 model (which is assumed throughout this work).

ACKNOWLEDGEMENTS

We would like to thank the anonymous referees for their useful comments and suggestions that we feel have greatly improved this manuscript. SMW and AB acknowledge support from the Science and Technology Facilities Council. WRC acknowledges support from an Institute of Physics/Nuffield Foundation funded summer internship at the University of Oxford. RACC thanks the Leverhulme Trust for their award of a Visiting Professorship at the University of Oxford. The simulations were run on the Cray XT5 supercomputer Kraken at the National Institute for Computational Sciences. This research has been funded by the National Science Foundation (NSF) PetaApps programme, OCI-0749212 and by NSF AST-1009781.

REFERENCES

Anders P., Fritze -v., Alvensleben U., 2003, A&A, 401, 1063
Bouwens R. J. et al., 2010a, ApJ, 708, L69
Bouwens R. J. et al., 2010b, ApJ, 709, L133
Bouwens R. J. et al., 2011, ApJ, 737, 90
Bouwens R. J. et al., 2012, ApJ, 754, 83
Bouwens R. J. et al., 2013, preprint (arXiv:1306.2950)
Bruzual G., Charlot S., 2003, MNRAS, 344, 1000
Bunker A. J. et al., 2010, MNRAS, 409, 855
Calzetti D., Armus L., Bohlin R. C., Kinney A. L., Koornneef J., Storchi-Bergmann T., 2000, ApJ, 533, 682
Coe D. et al., 2012, ApJ, 762, 32
Conroy C., Gunn J. E., 2010, ApJ, 712, 833
Di Matteo T., Colberg J., Springel V., Hernquist L., Sijacki D., 2008, ApJ, 676, 33
Di Matteo T., Khandai N., DeGraf C., Feng Y., Croft R. A. C., Lopez J., Springel V., 2012, ApJ, 745, L29
Ellis R. S. et al., 2013, ApJ, 763, L7
Eyles L. P., Bunker A. J., Stanway E. R., Lacy M., Ellis R. S., Doherty M., 2005, MNRAS, 364, 443
Finkelstein S. L., Papovich C., Giavalisco M., Reddy N. A., Ferguson H. C., Koekemoer A. M., Dickinson M., 2010, ApJ, 719, 1250
Finlator K., Oppenheimer B. D., Davé R., 2011, MNRAS, 410, 1703
Fioc M., Rocca-Volmerange B., 1997, A&A, 326, 950
Fioc M., Rocca-Volmerange B., 1999, preprint (astro-ph/9912179)
González V., Labbé I., Bouwens R. J., Illingworth G., Franx M., Kriek M., 2011, ApJ, 735, L34
Labbé I. et al., 2010, ApJ, 716, L103
Labbé I. et al., 2012, preprint (arXiv:1209.3037)
Lorenzoni S., Bunker A. J., Wilkins S. M., Stanway E. R., Jarvis M. J., Caruana J., 2011, MNRAS, 414, 1455
Lorenzoni S., Bunker A. J., Wilkins S. M., Caruana J., Stanway E. R., Jarvis M. J., 2013, MNRAS, 429, 150
Maraston C., 2005, MNRAS, 362, 799
McLure R. J. et al., 2013, MNRAS, 432, 2696
Oesch P. A. et al., 2010a, ApJ, 709, L16
Oesch P. A. et al., 2010b, ApJ, 709, L21
Oesch P. A. et al., 2012a, ApJ, 745, 110
Oesch P. A. et al., 2012b, ApJ, 772, 136
Oesch P. A. et al., 2013, ApJ, 773, 75
Oke J. B., Gunn J. E., 1983, ApJ, 266, 713
Pei Y. C., 1992, ApJ, 395, 130
Salpeter E. E., 1955, ApJ, 121, 161
Schenker M. A. et al., 2013, ApJ, 768, 196
Springel V., 2005, MNRAS, 364, 1105
Springel V., Hernquist L., 2003, MNRAS, 339, 289
Stanway E. R., McMahon R. G., Bunker A. J., 2005, MNRAS, 359, 1184
Stark D. P., Schenker M. A., Ellis R., Robertson B., McLure R., Dunlop J., 2012, ApJ, 763, 129 (S12)
Taylor E. N. et al., 2011, MNRAS, 418, 1587
Wilkins S. M., Bunker A. J., Ellis R. S., Stark D., Stanway E. R., Chiu K., Lorenzoni S., Jarvis M. J., 2010, MNRAS, 403, 938
Wilkins S. M., Bunker A. J., Lorenzoni S., Caruana J., 2011a, MNRAS, 411, 23
Wilkins S. M., Bunker A. J., Stanway E., Lorenzoni S., Caruana J., 2011b, MNRAS, 417, 717
Wilkins S. M., Gonzalez-Perez V., Lacey C. G., Baugh C. M., 2012, MNRAS, 424, 1522
Wilkins S. M., Bunker A., Coulton W., Croft R., Matteo T. D., Khandai N., Feng Y., 2013a, MNRAS, 430, 2885
Wilkins S. M., Gonzalez-Perez V., Baugh C. M., Lacey C. G., Zuntz J., 2013b, MNRAS, 431, 430

APPENDIX A: THE CHOICE OF THE SPS MODEL

A key ingredient in our analysis is the transformation of the simulated star formation and metal enrichment history into an SED through the use of SPS modelling. SPS models work by combining stellar tracks, which model different stellar evolution phases, with spectral libraries, which empirically or theoretically relate the spectral output to individual stars based on their mass, age and chemical composition. By combining these with a choice of IMF and initial chemical composition, it then becomes possible to model the SEDs of simple stellar populations.

However, due to differences in the treatment of stellar evolution and the utilized spectral libraries, SPS models produce varying results for the SEDs of stellar populations (see, for example, Conroy & Gunn 2010). An example of some of these differences can be seen in Fig. A1, where we show the SEDs of simple stellar populations with ages between 10 Myr and 10 Gyr predicted assuming three popular SPS models: PEGASE.2; BC03: Bruzual & Charlot (2003);

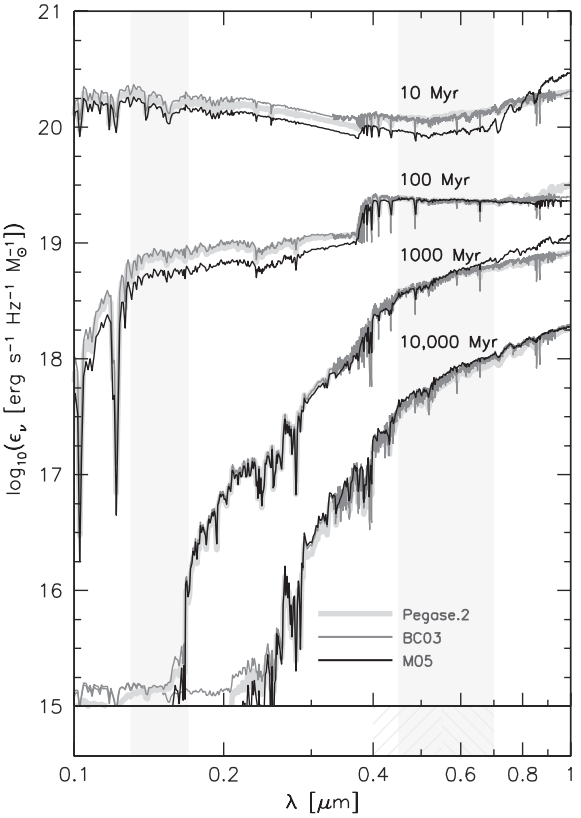

Figure A1. The pure stellar SED of simple stellar populations (with age $\in \{10, 100, 1000, 10\,000\}$ Myr and $Z = 0.02$) predicted by various SPS models. Each SED is normalized to have the same initial mass. The two vertical shaded bands denote the location and width of the 1500 and V_w filters considered in this work.

M05: Maraston (2005). For the youngest ages considered (10 and 100 Myr), there are significant differences between the models.

For older populations (>1 Gyr), the models are relatively consistent over the rest-frame UV–optical. In the near-IR however the M05 model predicts an excess of flux at 1 Gyr, attributed to a more detailed treatment of the thermally pulsing asymptotic giant branch (TP-AGB) stage. While this produces significant enhancement of the near-IR flux, it will have little effect on this work due to our focus on rest-frame UV–optical colours and very high redshift galaxies.

The variation between different SPS models, and its relevance to this work, can be seen more clearly in Fig. A2, where we show the evolution of the rest-frame stellar $1500 - V_w$ as a function of age for a simple stellar population (with $Z = 0.02$). While the BC03 and PEGASE.2 models yield a similar colour evolution, the M05 model predicts significantly redder colours at ages 10–500 Myr.

This variation between different models will then leave the colours predicted by our analysis of the *MassiveBlack*-II simulation sensitive to the choice of model. In Fig. A3, we show the predicted rest-frame stellar $1500 - V_w$ colour assuming various SPS models (cf. Fig. 10); the lower panel of this figure shows the difference

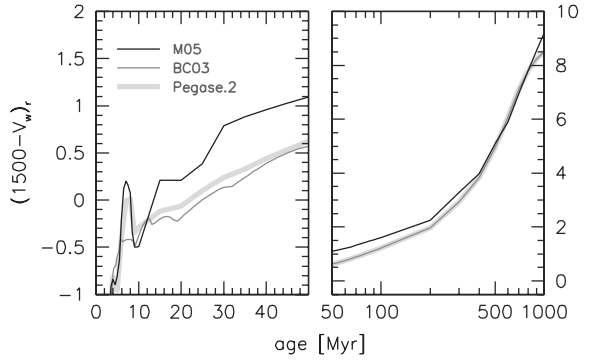

Figure A2. The evolution of the rest-frame stellar $1500 - V_w$ as a function of age for a simple stellar population ($Z = 0.02$) assuming the M05, BC03 and PEGASE.2 SPS models.

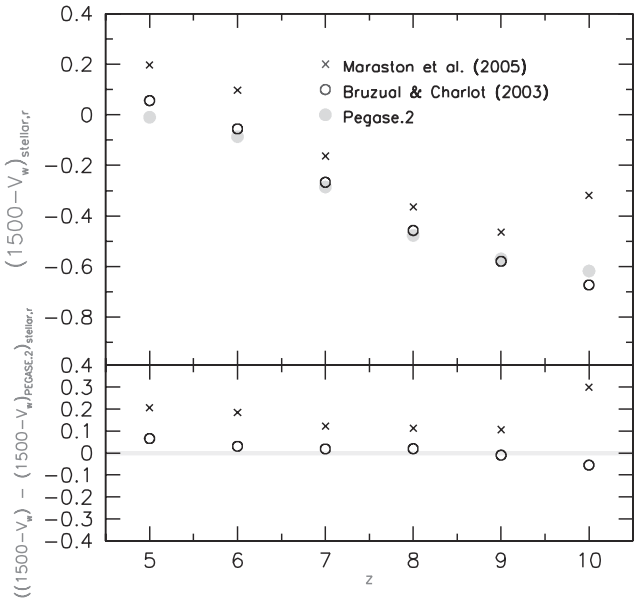

Figure A3. The median pure stellar intrinsic rest-frame $1500 - V_w$ colour of galaxies with $-20.5 < M_{1500} < -18.5$ at $z \in \{5, 6, 7, 8, 9, 10\}$ determined assuming various SPS models (cf. Fig. 10). The lower panel shows the difference between the default PEGASE.2 predictions and the M05 and BC03 model predictions.

between the alternative models considered and the PEGASE.2 model utilized throughout this work. While the use of the BC03 model yields colours similar (<|0.1| mag difference) to those assuming the PEGASE.2 (default) model, the M05 model yields colours which are typically between 0.1 and 0.2 mag redder. At the most extreme, the use of the M05 model at $z = 10$ yields colours ≈0.3 mag redder than using PEGASE.2.

This paper has been typeset from a TEX/LATEX file prepared by the author.